Measuring pKa of Activation and pKi of Inactivation for Influenza Hemagglutinin from Kinetics of Membrane Fusion of Virions and of HA Expressing Cells

Aditya Mittal,* Tong Shangguan,† and Joe Bentz*
*Department of Bioscience and Biotechnology, Drexel University, Philadelphia, Pennsylvania 19104 USA; and †Elan Corporation, 1 Research Way, Princeton, New Jersey 08540 USA

ABSTRACT The data for the pH dependence of lipid mixing between influenza virus (A/PR/8/34 strain) and fluorescently labeled liposomes containing gangliosides has been analyzed using a comprehensive mass action kinetic model for hemaglutinin (HA)-mediated fusion. Quantitative results obtained about the architecture of HA-mediated membrane fusion site from this analysis are in agreement with the previously reported results from analyses of data for HA-expressing cells fusing with various target membranes. Of the eight or more HAs forming a fusogenic aggregate, only two have to undergo the "essential" conformational change needed to initiate fusion. The mass action kinetic model has been extended to allow the analysis of the pKa for HA activation and pKi for HA inactivation. Inactivation and activation of HA following protonation were investigated for various experimental systems involving different strains of HA (A/PR/8/34, X:31, A/Japan). We find that the pKa for the final protonation site on each monomer of the trimer molecule is 5.6 to 5.7, irrespective of the strain. We also find that the pKi for the PR/8 strain is 4.8 to 4.9. The inactivation rate constants for HA, measured from experiments done with PR/8 virions fusing with liposomes and X:31 HA-expressing cells fusing with red blood cells, were both found to be of the order of 10^{-4} s^{-1}. This number appears to be the minimal rate for HA's essential conformational change at low HA surface density. At high HA surface densities, we find evidence for cooperativity in the conformational change, as suggested by other studies.

INTRODUCTION

Elucidation of influenza HA-mediated membrane fusion site architecture has been the focus of intense research since it was the first fusion protein whose crystal structure was solved (Wilson et al., 1981; Bullough et al., 1994) and its structure is related to other fusion proteins (Skehel and Wiley, 1998). Furthermore, it is the only membrane fusion system for which there is quantitative data that can be used to deduce how many fusion proteins are required at the fusion site (Bentz et al., 1990; Ellens et al., 1990; Melikyan et al., 1995; Danieli et al., 1996; Blumenthal et al., 1996; Bentz, 2000a; Mittal and Bentz, 2001). Thus, the architecture of its fusion site is being elucidated.

Recently, Bentz (2000a) began development of a comprehensive mass-action model for HA-mediated fusion to analyze the first fusion pore kinetics measured by Melikyan et al. (1995). The model was extended in Mittal and Bentz (2001) to extract consensus parameters for the data of Melikyan et al. (1995), Danieli et al. (1996), and Blumenthal et al. (1996) for HA-expressing cells fusing with various target membranes. The model includes a rigorous distinction between the minimum number of HA trimers aggregated at the nascent fusion site and how many of those trimers that must undergo a slow essential conformational change before the first conductivity can be measured across the fusing systems. This distinction allowed us to show that HAs bound to sialates on glycophorin could be members of the fusogenic aggregate but not undergo the essential conformational change needed to form the first fusion pore (Mittal and Bentz, 2001).

Assuming a nucleation model for HA aggregation, it was found that at least eight HAs must aggregate to form the fusogenic aggregate that results in initiating membrane fusion. This nucleation model is unlikely to accurately describe the true distribution of HA aggregates over the cell population, but it yields the minimum estimate for the number of HAs required to form the fusogenic aggregate. In other words, more realistic distributions would require that there are more than eight HAs in a fusogenic aggregate (Bentz, 2000a). Thus, the minimal aggregate size is $\omega = 8$, and of these, only two need to undergo the slow essential conformational change required to initiate fusion.

However, it remained to be shown the extent to which the results for HA-expressing cells were applicable to the virus fusing with target membranes. Further, the HA surface density on virions is reasonably constant (Ruigrok et al., 1984, 1985), so the noise associated with surface density heterogeneity in the data is negligible, as compared with the data of HA-expressing cells fusing with target membranes. Although the surface density of HA on virions cannot be reduced without causing surface density heterogeneity, we can homogeneously reduce the surface density of "active" HA by raising the pH. This approach was used by Doms et al. (1985) and Blumenthal (1988) to estimate the number of HAs required for fusion. Here we analyzed the kinetic data of the influenza virus fusing with the ganglioside GD1a

Submitted March 14, 2002, and accepted for publication June 27, 2002.
Address reprint requests to Joseph Bentz, 3141 Chestnut Street, Philadelphia, PA 19104-2875. Tel.: 215-895-1513; Fax: 215-895-1273; E-mail: bentzj@drexel.edu.

0006-3495/02/11/2652/15 $2.00

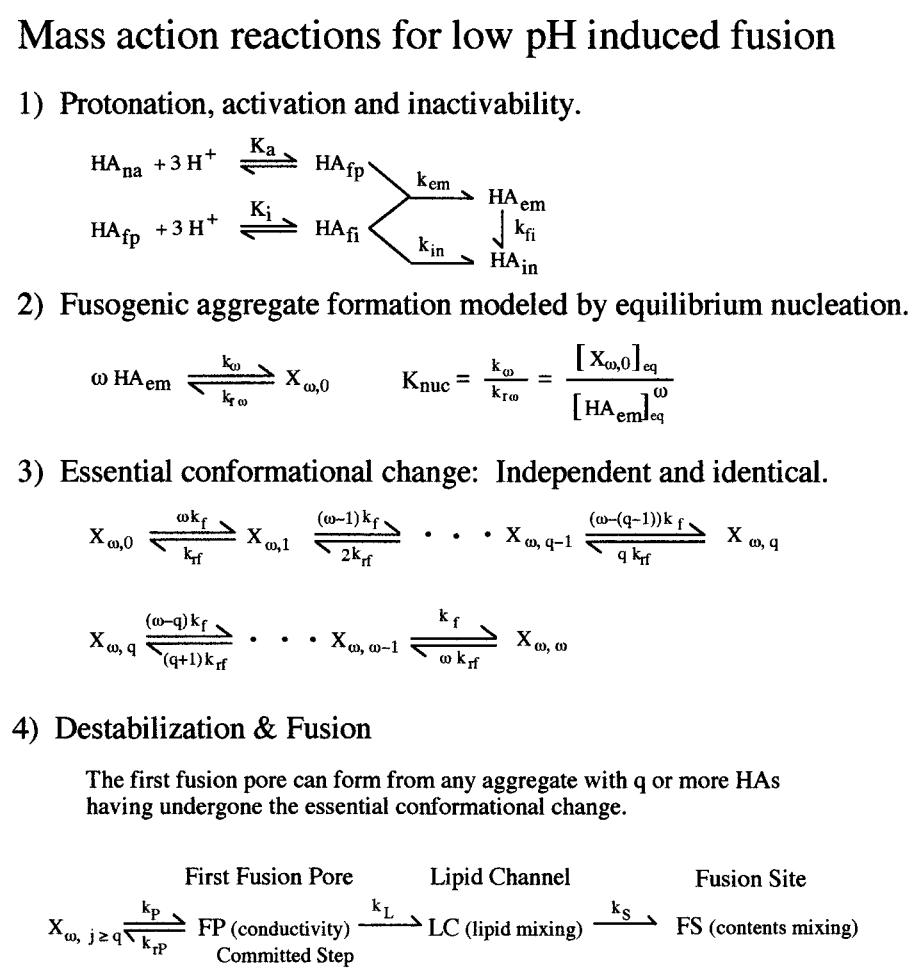

FIGURE 1 Comprehensive kinetic model for influenza hemagglutinin mediated membrane fusion. The protonation reactions shown in step 1 are assumed to occur instantaneously, relative to the protein conformational changes, and remain at equilibrium throughout the fusion process. Stoichiometrically, we are concerned only about the last protonation site for each of the monomers in the HA trimer. HA trimer in native form (HA_{na}) is protonated to expose the fusion peptide (HA_{fp}). According to the model proposed in Bentz (2000b) and extended in Bentz and Mittal (2000), the exposed fusion peptide embeds into the viral membrane (HA_{em}) or is further protonated to become an inactivable species (HA_{fi}). HA_{fi} can either inactivate directly resulting in HA_{in} (HA incapable of being a part of the fusion mechanism) or can proceed as a part of HA_{em} species. In principle, all HA_{in} derived from the HA_{em} species should come from HA_{fi} species. Step 2 represents nucleation aggregation that is at equilibrium, assumed to guarantee the smallest estimate for the number of HAs in a fusogenic aggregate. Following protonation, the HA_{em} aggregate of size ω forms rapidly denoted as $X_{\omega,0}$. ω is the minimal size for a fusogenic aggregate and a lower bound of eight was found by kinetic analysis in Bentz (2000a), i.e., $\omega = 8$. At step 3, ω denotes the number of the HAs within the fusogenic aggregate which can undergo the essential conformational change, independently and identically with a rate constant of k_f. Thus, the overall rate constant for the first reaction would be ωk_f. These conformational changes continue for each HA until q of them have occurred, $X_{\omega,q}$. q is called the minimal fusion unit, as it equals the minimum number of HAs that have undergone the essential conformational change needed to stabilize the first high energy intermediate for fusion. At step 4, the fusogenic aggregate can transform to the first fusion pore, which is observed as the first conductivity across the apposed membranes. The first fusion pore, FP, evolves to the lipid channel, LC, demarked by mixing of lipids, which evolves to the fusion site, FS, demarked by aqueous contents mixing.

containing liposomes from Shangguan (1995) and Shangguan et al. (1996, 1998). We find that the approach can estimate the number of fusogenic aggregates in the area of contact with the target membrane.

The mass-action model used in Mittal and Bentz (2001) has been extended here to include activation and inactivation kinetics following protonation of HA. We have analyzed the inactivation data for the A/PR/8/34 strain of HA in virions (Shangguan et al., 1998), the X:31 strain of HA expressed in cells (Leikina et al., 2000), and the pH-dependent activation data for Japan strain expressed in cells (Mittal et al., 2002).

KINETIC MODEL

The mass action kinetic model shown in Fig. 1 extends the previously published versions (Bentz, 2000a; Mittal and Bentz, 2001) by the addition of explicit protonation reactions to HA in step 1 of Fig. 1. It is well known that both

PR8 and X31 strains of the influenza virus show inactivation of fusion capacity when the pH is low enough (Nir et al., 1990; Duzgunes et al., 1992; Körte et al., 1997, 1999), and recently Markovic et al. (2001) have shown that Japan strain of HA can inactivate at high HA surface densities. The mechanism of this inactivation is not known, but to obtain reliable rate constants for fusion for these HAs, we must take this inactivation into account. The data of Korte et al. (1997, 1999) suggest that in addition to the protonation required for activation of HA, the protonation of a second site is required to allow HA inactivation of the PR8 and X31 strains. Obviously, there might be more than a single site on each HA monomer that must be protonated to initiate the conformational changes leading to fusion, just as more than one site might need to be protonated to initiate those conformational changes leading to HA inactivation. Here, we consider only the sites with the smallest pKs, i.e., the last sites to be protonated as the pH is lowered. Because HA is a homotrimer, we do assume three identical and independent protonation sites per HA, regardless of function. These protonation reactions are assumed to occur instantaneously, relative to the protein conformational changes, and remain at equilibrium throughout the fusion process. Both of these assumptions are reasonable. The equations governing these equilibrium reactions are shown in Appendix A.

We start with native HA at neutral pH (Fig. 1), denoted HA_{na}, which is first protonated to the fusion active form with the fusion peptide exposed, denoted HA_{fp}. If the pH is low enough, HA is protonated further to an inactivatible form, denoted HA_{fi}. Whether inactivatible HA does in fact inactivate will depend upon the pathway it follows, i.e., the relative rate constants. Both HA_{fp} and HA_{fi} can move to the next stage, wherein the fusion peptide is embedded into the proper membrane to initiate fusion, denoted HA_{em}. Whether that membrane is the viral membrane or the target membrane has been widely discussed, but is not germane to this analysis.

Inactivation is any conformational modification of HA after protonation that renders it nonfusogenic, denoted by HA_{in}. Therefore, in step 1 of Fig. 1, we assume that both species HA_{fp} and HA_{fi} can inactivate at different rates. Although not necessary for our kinetic analysis, it seems simplest to consider inactivation to be the fate of an HA, which undergoes the essential conformational change, either in absence of target membrane or in presence of a target membrane when that HA is not a member of a fusogenic aggregate (Bentz, 2000b; Bentz and Mittal, 2000). This latter designation would also include the case of having fusion inhibitors that do not interfere with HA conformational changes (e.g., lysophosphatidylcholine (LPC); Leikina et al., 2001). In this case, we would expect the rate of inactivation being measured, i.e., k_{fi}, should be similar to the rate of the essential conformational change, k_f, shown in step 3 of Fig. 1. We shall see that this is the case when HA surface density is low, while at higher surface densities, k_f shows some cooperativity. Whether the essential conformational change is the formation of the extended coiled coil, or the helix turn transition near the transmembrane (TM) domain of HA, or the interaction between the N cap region and the C-terminal residues adjacent to the TM domain, or yet some other change, has been widely discussed but is not germane to this analysis.

Since the subsequent steps of the mass action model shown in Fig. 1 have been discussed previously (Bentz, 2000a; Mittal and Bentz, 2001), we will describe them briefly here. In step 2 of Fig. 1, nucleation aggregation is assumed to occur rapidly, supported by the analysis in Bentz (2000a) and remain at equilibrium. The nucleation mechanism was assumed solely because it would predict the minimum number of HAs needed to form a fusion site. This minimal aggregate size is called a fusogenic aggregate, which has been fitted as $\omega = 8$ (Bentz, 2000a). This step will be very important in the analysis of inactivation kinetics, as described below. Other, more realistic distributions would yield larger numbers for the minimal aggregate size (Bentz, 2000a).

In step 3 of Fig. 1, the HAs within the fusogenic aggregate independently and identically undergo the essential conformational change. Once q of them have done so, in which q is the fitted parameter called the minimal fusion unit, then the fusogenic aggregate can form the first fusion pore (FP), as shown in step 4. Note that while $q \leq \omega$, it is otherwise independent of ω (Bentz, 2000a). The first fusion pore is measured by conductivity (Melikyan et al., 1995) or transmembrane electrostatic potential changes (Blumenthal et al., 1996). This transforms to a lipid channel (LC), monitored by the spread of fluorescent lipids (Shangguan et al., 1996, 1998; Danieli et al., 1996; Blumenthal et al., 1996; Chernomordik et al., 1997, 1998; Armstrong et al., 2000; Mittal et al., 2002). Finally, the fusion site (FS) can be formed, as monitored by aqueous contents mixing of fluorescent molecules (Blumenthal et al., 1996; Leikina et al., 2001; Mittal et al., 2002), provided there is not too much leakage of contents (Shangguan et al., 1996; Gunther-Aüsborn et al., 2000).

Because this kinetic model has many reactions, each of which is necessary to adequately represent the fusion process, it is helpful to see how the important species in the model behave over time. Fig. 2 shows a theoretical simulation for lipid mixing (LC formation in the mass action model in Fig. 1, all steps) using cells constants for the HAb2 cells fusing with RBCs and typical rate constants, based on our previous work (see figure legend). The arrows show time points for start and end of the lipid mixing respectively. Fig. 3 shows (on a logarithmic scale, since rate constants vary widely in magnitude) the number of activated/embedded HAs, HA_{em}, and number of fusogenic aggregates, N_ω, in the area of apposition during the simulation time of Fig. 2.

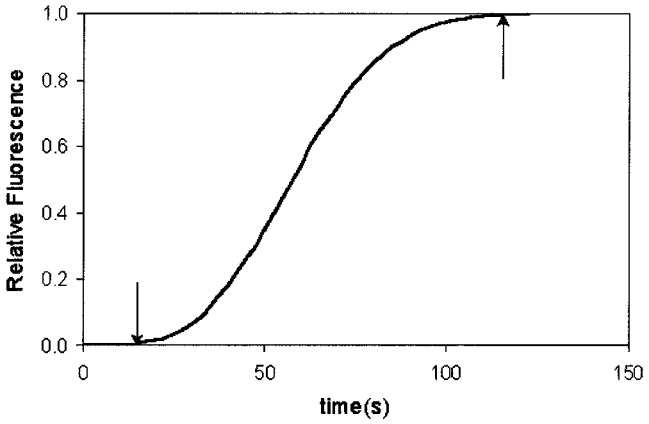

FIGURE 2 Simulated curve for lipid mixing for HAb2 cells fusing with RBCs at pH 4.9 using the kinetic model in Fig. 1. Arrows indicate the start and end of the lipid mixing process. Values for parameters of Fig. 1 were fixed as following, based on our previous and current work: pKa = 5.7, pKi = 4.8, $k_{em} = 1\ s^{-1}$, $k_{in} = 1\ s^{-1}$, $k_{fi} = 2 \times 10^{-4}\ s^{-1}$, $\omega = 8$, $q = 2$, $k_f = 1 \times 10^{-2}\ s^{-1}$, $k_p = 5 \times 10^{-4}\ s^{-1}$, $k_1 = 3 \times 10^{-2}\ s^{-1}$.

Fig. 3 shows that the number of activated, embedded HAs reaches a steady state in a few seconds, and the number of fusogenic aggregates reaches a steady-state value soon thereafter. The lipid mixing is observed during the steady-state regime of the number of fusogenic aggregates, as shown by the arrows that correspond to the same time points as those in Fig. 2. The lipid mixing starts well after the onset of the steady-state phase of N_ω, and this explains why the dependence of initial rates or lag times on HA surface density cannot predict how many HAs compose the fusogenic aggregate (Bentz, 1992; Mittal and Bentz, 2001). The

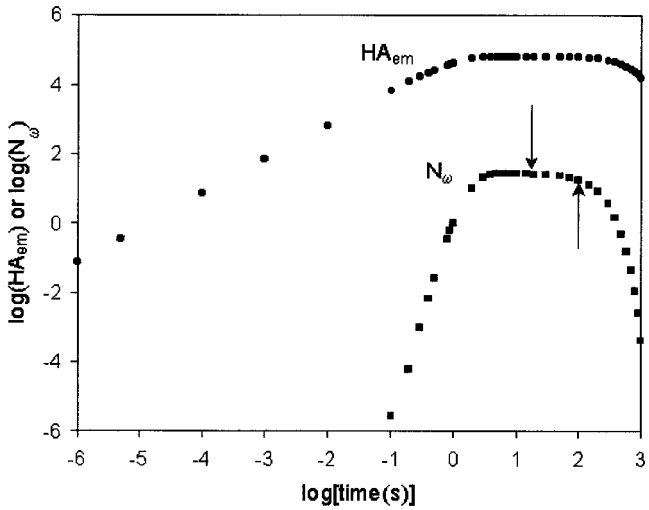

FIGURE 3 Numbers of the HA_{em} and the fusogenic aggregates, N_ω, in the area of apposition as a function of time during the lipid mixing observed in Fig. 2. Log-log plot is used for convenience. The parameter values were the same as used in Fig. 2, and changing these values do not affect the final outcome.

fact that N_ω is at steady-state value during the entire lipid mixing phase greatly simplifies the application of the model to the data, as will be explained in Materials and Methods.

To understand activation/inactivation of different strains of HA, Markovic et al. (2001) used an experimental protocol in which two low pH pulses were used. A low pH activation pulse was followed by reneutralization and binding of RBCs to HA-expressing cells for 15 min. At this stage, a second low pH pulse was required to start fusion. The kinetic model described here simply assumes that each HA, once protonated, is irreversibly committed to fusion or inactivation (see Eq. 3 below). The data being fit either have continuous low pH (Shangguan, 1995), did not require a second low pH application (Leikina et al., 2000), or all protonated HA continue to inactivate at neutral pH, during target membrane binding (Shangguan et al., 1998). For a system or protocol that requires a second pulse, that step could be added to the model.

MATERIALS AND METHODS

Virus-liposome fusion experiments

All of the data were recalibrated from original data as described below. Shangguan (1995) and Shangguan et al. (1998) grew influenza A/PR/8/34 (H1N1) virions in fertilized chicken eggs. The virions purified had normal infectivity. These virions were fused with NBD/Rh or CPT/DABS labeled DOPC/GD1a (90:10) LUVs having a diameter of 0.1 μm, approximately the same size as the virus. Stoichiometry of the fusion system was calibrated to be approximately one virion per liposome. The virus and liposomes were preincubated at 4°C for 30 min at neutral pH before the fusion reaction to start from prebound virion-liposome complexes (Shangguan et al., 1996). A small aliquot of the prebound virus-liposomes was transferred to a preequlibrated, thermostatted cuvette at 37°C to yield 10 μM viral phospholipid and 10 μM liposomal lipid. Lipid mixing was initiated by injecting concentrated acetic acid to the desired pH and measured by increase in fluorescence due to dilution of the probes into the viral envelope, assayed on PTI Alphascan fluorometer (South Brunswick, NJ). Lipid mixing from the prebound virion-liposome aggregates was first order, and no dissociation occurred within the time scale of the experiment (Shangguan et al., 1996).

Data calibration for the virus fusing with liposomes

Lipid mixing assay results were expressed originally in Shangguan (1995) and Shangguan et al. (1998), in terms of fluorescence dequenching, using a standard normalization,

$$I(t) = \frac{F(t) - F(0)}{F(\mathrm{det}) - F(0)} \qquad (1)$$

in which $F(t)$ and $I(t)$ represent the absolute and relative fluorescence intensities respectively at time t or time 0, and $F(\mathrm{det})$ is the fluorescence due to detergent ($C_{12}E_8$) lysis at the end of the experiment. To transform the cuvette dequenching data to equivalent waiting time distribution data, for applying the kinetic model, we recalibrated the intensity curves by replacing $F(\mathrm{det})$ with $F(\infty)$ in Eq. 1, which is the maximum possible probe redistribution due lipid mixing only, i.e., not due to detergent lysis. $F(\infty)$ is the plateau value of lipid mixing fluorescence and was found as described

previously (Mittal and Bentz, 2001). The new intensity data scaled from 0 to 1 was fitted to the kinetic model using the equation:

$$I(t) = N_L(t)[2 - N_L(t)] \quad (2)$$

in which $N_L(t) = 1 - \exp[-\{LC(t)\}]$, is the fraction of virions with one or more lipid mixing sites. This transformation of fluorescence dequenching intensity to equivalent cumulative waiting time distribution was derived in Mittal and Bentz (2001).

Algorithm for multiparameter fitting

Direct fits using the entire mass action model shown in Fig. 1 were too expensive computationally. Given that the absolute number of fusogenic aggregates, N_ω, is constant (at steady state) during the period of lipid mixing (shown in Figs. 2 and 3), it is reasonable to fit N_ω at its steady-state value, together with the fusion rate constants. Then we can fit the "protonation" parameters (step 1 in Fig. 1) to achieve this value of N_ω.

Furthermore, we have found that comprehensive kinetic analyses of HA-expressing cells (with varying surface densities of HA) fusing with planar bilayers and erythrocytes with steps 2, 3, and 4 of Fig. 1 provide an extremely robust measurement of the relative number of fusogenic aggregates for different HA cell lines (Bentz, 2000a; Mittal and Bentz, 2001). Therefore, we compartmentalized the fitting problem into two steps.

First, the kinetic curves for lipid mixing measurements (i.e., LC formation in step 4) were fit to steps 3 and 4 of Fig. 1 to give us reliable estimates for the steady-state number of fusogenic aggregates, N_ω, as a function of pH, along with the rate constants k_f, k_p, and k_1. Note that from step 4 in Fig. 1, $N_\omega = \delta X_{\omega,0}$ is the steady-state number of fusogenic aggregates in the area of contact, δ, of the fusing membranes. Because we have found that $\omega \geq 8$ and that the fits are fairly insensitive to larger values of ω (Bentz, 2000a; Mittal and Bentz, 2001), we have set $\omega = 8$ for the fittings done here.

Second, we exhaustively fitted the relative numbers of fusogenic aggregates we obtained as a function of pH, using steps 1 and 2, to obtain protonation and/or inactivation parameters, pKa, pKi, k_{em}, and k_{in}, depending on the experimental set up.

Screening for "best fits" from exhaustive fitting of the virus-liposome fusion

Numerical integrations for the mass action kinetic model were done as in Bentz (2000a) using MATLAB (The Math Works) subroutine ODE23s. Curve fitting was done using the fitting routine fminsearch, by minimizing the total root mean squared error (rmse) between all the numerically integrated values and the actual data values at each time point. A minimum rmse value for each data set was obtained, and "best fits" were defined as all sets of parameters that were visually indistinguishable from that of the minimum rmse fit. All data-fitting was exhaustive, i.e., the widest possible ranges of initial estimates for the parameters being fitted were tested to assure that all best fits were found.

For the lipid mixing data between virus and liposomes at different pH values (shown in Fig. 4), we attempted to fit all the seven curves simultaneously, however, this proved extremely expensive computationally. Hence, we devised a three-step process to fit the data.

First, the data at pH 4.84 and 4.9 were fitted jointly over all relevant parameters and rate constants, and a best-fit cutoff value of rmse $= 1.60 \times 10^{-2}$ was chosen, with an absolute minimum rmse of 9.52×10^{-3}. This yielded the best-fit kinetic constants (i.e., q, k_f, k_p, k_1) and the number of fusogenic aggregates N_ω (pH 4.9) and N_ω (pH 4.84). Because these two curves were central, the model was given maximum freedom to extract the differences between these curves.

Second, for each of these best fit parameter sets, data for each of the other pH values were fitted solely for the number of fusogenic aggregates, N_ω (pH), in the area of contact. This was reasonable because the number of fusogenic aggregates was at steady state during the lipid mixing time domain as described above. The combined best-fit rmse value, calculated by adding all individual rmse values obtained from each individual fitting, was found to be $= 9.88 \times 10^{-2}$, with an absolute minimum rmse $= 7.23 \times 10^{-2}$. The third step was to exclude those fits for which N_ω (pH 5.01) < 1, i.e., only those fits were included for which at least one fusogenic aggregate was found at the highest pH tested, which provided lowest number of possible activated HAs and hence the lowest number of available fusogenic aggregates.

It is important to mention here that the screening of best-fits would be unaffected by the choice of fitting the data at any two particular pH values in the first step. Our second step ensures that we screen the best-fits based on the data of all the pH values. Starting from data at any other pH values in the first step would yield the same results after the third step, with much more computational cost, since resolving the separation between the two central curves is critical.

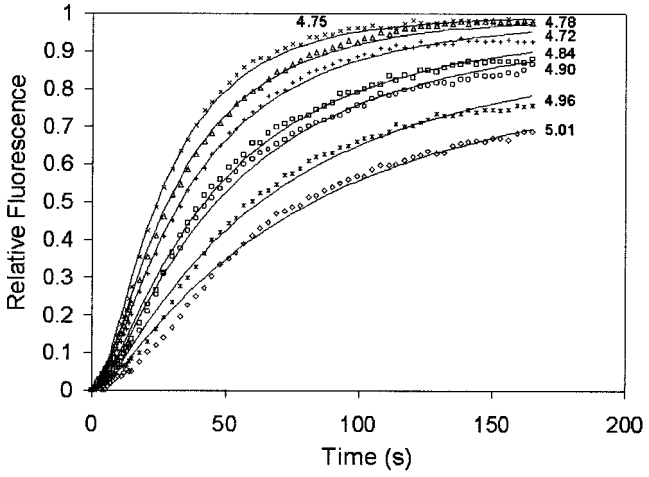

FIGURE 4 Disconnected symbols show pH dependence of influenza A/PR/8/34 virus lipid mixing. Concentrated (25×) unlabeled virus and NBD/Rh-labeled DOPC/GD1a (90:10) liposomes were mixed and preincubated at 4°C for 30 min to allow binding. A small aliquot of the prebound virus-liposomes was transferred to the pre-equilibrated cuvette at 37°C to yield 10 μM viral phospholipid and 10 μM liposomal lipid. Lipid mixing was initiated on lowering the pH to the indicated values (next to each curve) by injecting concentrated acetic acid. Solid lines show a typical best fit obtained from simultaneous multiparameter fitting of all the data to steps 3 and 4 of the kinetic model shown in Fig. 1. The parameters yielding best fits are shown in Table 1.

X31 HA expressing cells—RBC fusion experiments

We used data from Leikina et al. (2000) here to further study inactivation kinetics of HA. They used HA300a cells, which are CHO-K1 cells expressing the X:31 strain of influenza HA, fusing with PKH26 labeled RBCs. HA cells with bound RBCs at room temperature were treated with a 5-min pulse of pH 4.9 in the presence of 230 μM lauroyl lysophosphatidylcholine, LPC. The low pH medium was then replaced with LPC-containing phosphate-buffered saline (PBS) at neutral pH either without or with 0.5 unit/mL neuraminidase, respectively. After 5 min, the medium was replaced again by LPC-containing neuraminidase-free PBS. After different time intervals, LPC was removed by washing cells with LPC-free PBS, and lipid mixing was measured as PKH26 redistribution from RBC to HA cells (see Experimental Methods in Leikina et al., 2000).

Japan HA expressing cells—RBC fusion experiments

Mittal et al. (2002) used HAb2 cells expressing HA of Japan strain (A/Japan/305/57) fusing with R18 labeled RBCs at room temperature (20-22°C). Expressed HA0 at the cell surface was cleaved into its fusion-competent HA1-S-S-HA2 form with 10 μg/mL trypsin for 15 min at room temperature. The reaction was terminated by washing cells twice with the complete medium. Cells were washed twice by PBS and then incubated for 15 min with a 1-mL suspension of RBCs or RBC ghosts (0.05% hematocrit). The unbound RBCs were removed by three washings with PBS. HA-expressing cells with bound RBCs (~0-2 erythrocytes per cell) were then used for experiments. Fusion of HAb2 cells with RBCs labeled by membrane dye R18 was triggered by application of the low pH medium (PBS titrated by citrate to acidic pH supplemented with 1 mM *n*-propyl gallate), and assayed with fluorescence microscopy to find out the onset of dye redistribution for individual RBC-HA expressing cell pairs. Results are expressed as a cumulative distribution for fraction of cells showing lipid mixing at a given time.

Fitting inactivation kinetics for the PR8 and X31 strains of HA

Inactivation kinetics data are in form of the extent of lipid mixing after a preincubation time, t_{in}, in which HA can undergo conformational changes (e.g., low pH), but fusion is blocked. In Shangguan et al. (1998), fusion was blocked since there was no target membrane during the preincubation. In Leikina et al. (2000) RBCs were bound to cells, but fusion was blocked by LPC in the medium. They used the same low pH (4.9) for 5 min with LPC containing medium in these experiments, and assayed fusion after removing LPC at different time points, at neutral pH. Therefore, after the 5 min of preincubation in presence of LPC, the system has the same amount of HA_{em} to begin with for subsequent inactivation/fusion reactions.

For applying the kinetic model to these experiments, we focused on just the inactivation kinetics of the process and used the simplification of two irreversible paths:

$$\begin{array}{l} HA_{em} \xrightarrow{\text{Nucleation}} \text{Fusion} \\ \downarrow k_{fi} \\ HA_{in} \end{array} \qquad (3)$$

where, "Fusion" represents steps 3 and 4 of (Fig. 1) after formation of the fusogenic aggregate. When fusion is blocked, HA_{em} inactivate to HA_{in}. When the block is removed, the reaction in the fusion direction can proceed, given the remaining number of HA_{em}. Thus, the number of fusogenic aggregates will be reduced. Once $N_\omega < 1$ due to inactivation, there will be no subsequent fusion. The simplification of the mass action reactions in Fig. 1 shown by Eq. 3 are derived in Appendix B.

For fitting the inactivation kinetics data, the approach was similar to the second step of multiparameter fitting explained above. Given the extents of lipid mixing after individual preincubation times, we calculated the number of fusogenic aggregates, N_ω, by fixing the other fusion parameters (ω, q, k_f, k_p, k_1) at consensus values obtained from the multiparameter exhaustive analyses of each experimental system (Mittal and Bentz, 2001). Therefore, we obtained the N_ω that would give a particular extent of lipid mixing. Lower extents result from smaller N_ω values. Lower N_ω values are a result of HA_{em} inactivating via the k_{fi} pathway, Eq. 3. Thus, the decrease in N_ω values resulting from inactivation was fitted for k_{fi} using the nucleation reaction (step 2, Fig. 1). This fitting was done by normalizing the N_ω value for each extent of lipid mixing with the N_ω value of the control experiment for each system (e.g., no preincubation at low pH was the control experiment for Shangguan et al., 1998). With this protocol, the actual values of HA_{em} (to begin with after instantaneous protonation) and K_{nuc} were not required. Moreover, the ratio of fusogenic aggregates is a very robust parameter (Bentz, 2000a; Mittal and Bentz, 2001) and is not affected much by absolute values of fusion rate constants (k_f, k_p, k_1).

Virus and cell constants

For all calculations, 500 HA were assumed per virion and diameter of the virus was taken as 0.1 μm (Shangguan et al., 1998). Virus-liposome contact area was taken as 1/12th of the total surface area of the virus (we note that values of 1/10th, 1/8th, 1/6th, and 1/4th were also tested, but did not significantly affect the final outcomes of the calculations). Wherever applicable, the surface densities of HA on the HAb2 cells was taken as 2.56×10^3 HA/μm^2 (Ellens et al., 1990; Danieli et al., 1996). Total area of HA-expressing cells was taken as 2500 μm^2 (Ellens et al., 1990). Area of contact between a single RBC and HA-expressing cell was taken as 38 μm^2 (Danieli et al., 1996). We used 10^{-2} (molecules/μm^2)$^{-1}$ as the value for HA-glycophorin binding constant and assumed 8000 glycophorins per μm^2 on a RBC (Leikina et al., 2000; Mittal and Bentz, 2001).

RESULTS

The open symbols in Fig. 4 show fluorescence dequenching due to lipid mixing for influenza virus (A/PR/8/34) fusing with GD1a liposomes at indicated pH values. The solid lines show a best-fit to these data using Eq. 2, and all sets of best fit kinetic parameters gave visually indistinguishable curves. Over 6000 widely separated initial conditions were provided for fitting these data, i.e., the fitting was exhaustive. For all fittings, the only parameter that was fixed was $\omega = 8$ as explained in Materials and Methods. We note that higher values of ω do not make a significant difference (e.g., $\omega = 12$) as tested by us previously (Bentz, 2000a; Mittal and Bentz, 2001).

Table 1 summarizes the fitted parameters for the data. Whereas other values of the minimal fusion unit, q, could fit the data shown in Fig. 4, only $q = 1$ or 2 could best fit the data. Because there are many data sets here, it is difficult to clearly show a comparison between best-fit curves and minimum obtainable root mean squared values for other values of q, as was done in Fig. 3 of Bentz (2000a) for only two curves. Fig. 5 shows the difference in the experimental data (as per Eq. 1 with F(det) replaced by $F(\infty)$; see Materials and Methods) and the theoretically fitted values of relative fluorescence calculated (as per Eq. 2). Solid line represents the difference for $q = 2$ at pH 4.9, corresponding to the best-fits. This difference curve looks the same for the best fit with $q = 1$. The root mean squared error corresponding to this difference was $\leq 1.6 \times 10^{-2}$. Dashed line shows the difference between the data and the theoretical values for the minimum value of root mean squared error obtained with $q = 3$ with the root mean squared error corresponding to this difference being $\geq 2.0 \times 10^{-2}$. The deviation between the fitted values and the data is clearly worse for the dashed line as compared with the solid line. This deviation looks similar to or worse than the dashed line for other values of $2 < q \leq \omega$. The difference plots at all the other pH values show the same results as shown by Fig. 5.

TABLE 1 Fitted parameters for the data

Fusion system	q*	Protein k_f (s^{-1})†	FP k_p (s^{-1})†	LC k_1 (s^{-1})†	pKa‡	pKi‡
Virus (A/PR/8/34)-GD1a liposomes	1	1.0×10^{-2}	5.4×10^{-3}	3.9×10^{-1}	5.6–5.7	4.8–4.9
	2	3.0	5.4×10^{-3}	1.5×10^{-1}		
HAb2 cells (A/Japan/305/57)-RBCs	2	1×10^{-2}	5×10^{-4}	3×10^{-2}	5.6–5.7	n.d.

*, q denotes the minimal fusion unit. Only $q = 1$ or 2 could best fit the data for virus fusing with liposomes. ω, the minimal aggregate size, was fixed at 8 from Bentz (2000a). For the data of HAb2 cells fusing with RBCs, $q = 2$ from Mittal and Bentz (2001).

†, Best fit values for the rate constants for the essential conformational change of HA, k_f, the first fusion pore formation, k_p, and the lipid channel formation, k_1. Rate constants for HAb2 cells fusing with RBCs were fixed based on table 2 of Mittal and Bentz (2001).

‡, pKa denotes the pK of activation of HA (i.e., pH at which 50% of HA is activated) and pKi denotes the pK of inactivation of HA (i.e., pH at which 50% of HA is inactivated).

It is worth noting that fitting all the data in Fig. 4 simultaneously and selecting the best-fit parameter sets yielded only two convergent solutions for parameters, as opposed to ranges for parameters found in our previous work (Bentz, 2000a; Mittal and Bentz, 2001). This is due to the fact that the number of curves being screened simultaneously in our analysis was large. Bentz (2000a) fitted two curves (HAb2 and GP4f cell lines) and found robust estimates of the kinetic parameters in reasonably tight ranges.

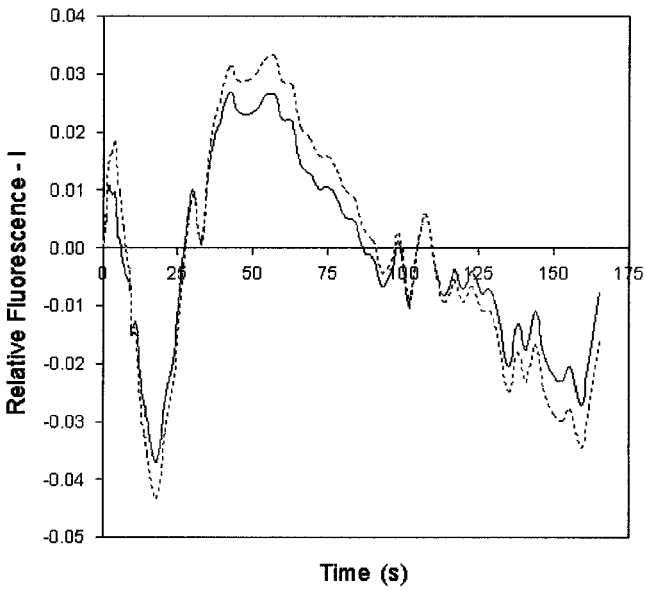

FIGURE 5 Only $q = 1$ or 2 could best fit the data. Solid line shows the difference in the experimental data (as per Eq. 1 with F(det) replaced by $F(\infty)$; see Materials and Methods) and the theoretically fitted values of relative fluorescence calculated as per Eq. 2, for $q = 2$ at pH 4.9, corresponding to the best fits. The difference was calculated by simply subtracting the theoretical values (represented by "I" in Eq. 2) from the experimental relative fluorescence values at each time point. This difference curve is same for the best fit with $q = 1$. The root mean squared error corresponding to this difference was $\leq 1.6 \times 10^{-2}$. Dashed line shows the above difference between the data and the theoretical values for the minimum value of root mean squared error obtained with $q = 3$. The root mean squared error corresponding to this difference was $\geq 2.0 \times 10^{-2}$. The deviation of theoretically calculated values from the data is clearly worse for the dashed line as compared with the solid line. This deviation looks similar to or worse for other values of q.

Mittal and Bentz (2001) fitted three curves (HAb2, GP4f, and GP4/6 cell lines) and found tighter ranges. Here, we fitted seven curves, and the best-fit values obtained for the kinetic parameters were narrowed down to just two converging solutions.

A major point of our analyses is the assumption that all the fusion data sets analyzed are reasonable, which implies that the subset of parameters that best fit all the different data sets are the most reliable. This subset is defined as consensus best fits from all the data. This implies that the consensus value for the minimal fusion unit is $q = 2$ (Bentz, 2000a; Mittal and Bentz, 2001). For the rate constants, we find strain dependent differences, which is not surprising.

For virions fusing with liposomes, the estimated value of k_f, the rate constant for the HA essential conformational change, is 3 s^{-1} when $q = 2$, which is faster than what we had found previously with Japan HA expressing cells fusing with target membranes. Whereas the strain difference may explain a part of this difference, it is consistent with our previous observation that increasing HA surface density seems to give a faster k_f value (see Table 1 here and Tables 1 and 2 in Mittal and Bentz (2001)). This is an indication of true "cooperativity" during HA mediated fusion, which we will discuss further below.

The estimated ranges for average rate constants for the first fusion pore formation (k_p) and the lipid channel (k_1) formation during virus-liposome fusion are 10 times faster than what we obtained previously for HA expressing cells fusing with various target membranes. There is clearly a difference between PR8 virions and Japan-HA expressing cells fusing with different target membranes.

"pK" for activation and inactivation of HA from influenza A/PR/8/34 virus

It is obvious from the data in Fig. 4 that viral inactivation occurs at the lower pH values. In Fig. 6, we plot the absolute values for N_ω that were obtained from the first step of the multiparameter fitting algorithm as a function of pH, as shown by solid circles. From these values of fitted N_ω, we can estimate the pKa for HA activation and pKi for HA inactivation using a Henderson-Hasselbach equation for a

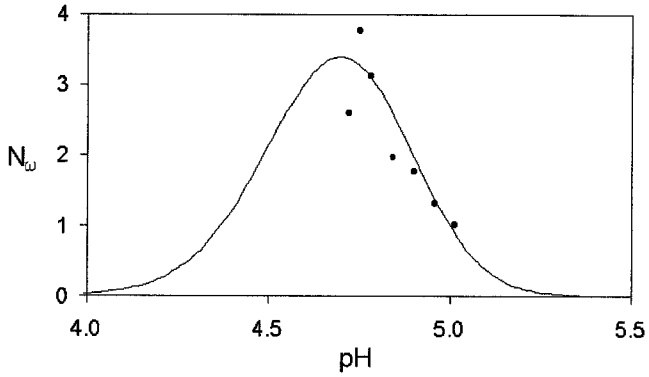

FIGURE 6 Number of fusogenic aggregates in the contact area between the influenza A/PR/8/34 virus and liposomes as a function of pH. Solid circles are the number of fusogenic aggregates obtained at different pH values by the multiparameter fitting shown in Fig. 4. The smooth curve shows a multiparameter fit of the number of fusogenic aggregates using steps 1 and 2 of the kinetic model shown in Fig. 1. A pKa of 5.6 to 5.65 was obtained for the last protonation site responsible for "activation" on each of the HA monomers of a HA trimer. A pKi of 4.8 to 4.9 was obtained for the protonation site on each monomer responsible for "inactivating" the trimer of HA. At pH $<$ pKi $-$ 1 = 3.8, the number of fusogenic aggregates should theoretically be zero, since all HA are inactivated. Indeed that is the case, as seen by extrapolating the pH dependence of number of fusogenic aggregates, shown by the smooth curve.

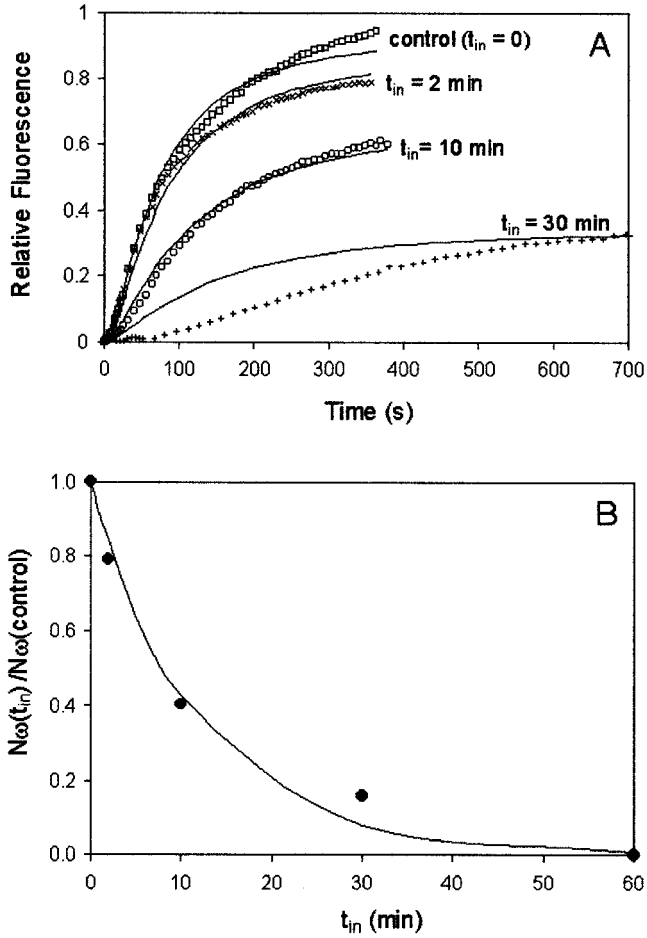

FIGURE 7 Inactivation of influenza PR/8 virus at 30°C measured by Shangguan et al. (1998). Unlabeled virus was incubated alone at 30°C, pH 4.9, for the indicated time in minutes shown next to each curve. At the end of each incubation period, virus was injected into cuvettes containing CPT/DABS-labeled DOPC/GD1a (90:10) liposomes at neutral pH. Lipid mixing was initiated after 50 s by acidification. (*A*) Symbols show the measured lipid mixing kinetics. Solid lines show fits to the data using steps 3 and 4 of the kinetic model shown in Fig. 1, to obtain the number of fusogenic aggregates at the start of lipid mixing for each pH value. The values of fusion parameters (see Eq. 7 here) were fixed at the values shown in Table 1. (*B*) Simultaneous fitting of the data in *A* gave number of fusogenic aggregates as a function of time of incubation of the virus alone at pH 4.9. To investigate inactivation of HA as a function of this time of incubation, we normalized the number of fusogenic aggregates for each time of incubation to control (which corresponds to the number of fusogenic aggregates at pH 4.9 without any preincubation of the virus alone), shown by solid circles. The normalized number of fusogenic aggregates was fitted to obtain the rate of conformational change for inactivation of HA, k_{fi}, shown by the smooth curve. Shangguan et al. (1998) found no lipid mixing when the virus was preincubated at pH 4.9 for 60 min, therefore, we took the number of fusogenic aggregates for that data as zero.

trimer of sites, as shown in Appendix 1. The pH dependency of fusogenic aggregates was exhaustively fitted with the inactivation mass-action shown in step 1 of Fig. 1 using Eqs. A.10, B.1, and B.2. All best fit solutions were visually similar to the one shown in Fig. 4 and gave pKa for HA activation as 5.62 $\pm$ 0.01 and pKi of HA inactivatibility as 4.87 $\pm$ 0.02 ($n > 50$). These appear to be conclusive fits.

The rate constants obtained were $k_{em} = 0.1\ s^{-1}$ and $k_{in} = 1\ s^{-1}$. These values for rate constants are in accord with Bentz (2000a), where it was explicitly shown that fusion is not rate limited by HA aggregation. The calculated K_{nuc} values were within a very narrow range of 2 to 5 $\times\ 10^{-11}$ (molecules/μm^2)$^{-7}$. Here the most important parameters that we were able to find were the pKa and pKi for HA of the influenza PR/8 virus. According to Eq. A.10, with pKi = 4.8 only 16% of the HAs are inactivatible at pH 4.72. These pK values reflect the requirement that all the three sites on the HA trimer must be protonated for it to be activated or inactivatible, which requires a lower pH than for just protonating a monomer.

Inactivation kinetics of influenza A/PR/8/34 virus

Symbols in Fig. 7 *A* show the data from Shangguan et al. (1998) for preincubation of the virus alone at pH 4.9 for the indicated times (t_{in}) before addition of ganglioside (10 mol%) containing liposomes. Solid lines show fits to the data using steps 3 and 4 of Fig. 1, fitted only for the number of fusogenic aggregates for each data set. Other fusion parameters (q, k_f, k_p, k_1) were fixed from Table 1 as our aim was to find out the number of fusogenic aggregates that could possibly give the extent of lipid mixing. Morphological observations (cryo-EM) of the virus after 30 min of incubation at pH 4.9 showed substantial morphological

changes in the virus in Shangguan et al. (1998), which may explain why the initial fit to that data is not very good for the curve with $t_{in} = 30$ min. However, as stated above, we can model the number of fusogenic aggregates that could possibly give the extent of lipid mixing reached for that particular curve (i.e., for $t_{in} = 30$ min), so for our purposes here, fitting the final part of the curve was most important.

Because we deal with ratios of fusogenic aggregates for our calculations (see Materials and Methods), actual values of HA_{em} at the start of fusion measurements are not required. Using Eq. B.4 in Eq. B.2 allows us to fit for k_{fi} as shown in Fig. 7 *B*, where solid circles represent the measured ratios of fusogenic aggregates, and the smooth curve shows the fit, giving us $k_{fi} = 1.8 \times 10^{-4}\ s^{-1}$.

Inactivation kinetics of X:31 strain of influenza HA

Leikina et al. (2000) measured extents of fusion after arresting fusion, between HA300a cells (expressing X:31 strain of HA) and PKH26-labeled RBCs, with LPC for different times. The idea was to investigate inactivation kinetics of HA by allowing HA to undergo whatever conformational changes during (and after) application of low pH (4.9) for 5 min and not allowing fusion to proceed by addition of LPC during the pH 4.9 application. After 5 min of preincubation with the HA in an activated or inactivatible form, LPC in neutral medium prevented any fusion for various times. Once LPC is removed, only the remaining activated HA can mediate fusion. Further, the experiments were done with and without addition of neuraminidase, to investigate the possible role of HA bound to sialates on glycophorins.

We were able to apply our Eqs. B.2 to B.4 for their experimental system also. First, we calculated the number of fusogenic aggregates required to give the extents shown in figure 2 of Leikina et al. (2000). This was done by fixing the fusion parameters (q, k_f, k_p, k_1) to the values for HA expressing cells fusing with erythrocytes shown in Table 1. The solid symbols in Fig. 8 show the ratio of the number of fusogenic aggregates corresponding to the extents measured by Leikina et al. (2000) relative to the control. The application of Eq. B.2 to data shown in Fig. 8 was straightforward. When LPC is present in the medium, HA_{em} will not contribute to fusion and will inactivate via k_{fi} pathway to give HA_{in}. This way, we fit the solid symbols in Fig. 8 for k_{fi} using Eqs. B.2 and B.4. However, before doing this, we had to consider that HA bound to glycophorin cannot undergo the essential conformational change for fusion (Leikina et al., 2000; Mittal and Bentz, 2001). Therefore, we needed to actually apply the fact that the species HA_{em} capable of conformational changes for either fusion or inactivation in our model was coming only from the free HA in the area of contact. In Appendix B, we have shown the equations required to calculate this effect of this HA-glycophorin binding (Eqs. B.5–B.7). Note that Eq. B.7 is of exactly the same form as Eq. B.2 with the incorporation of HA-glycophorin binding effects on the calculations.

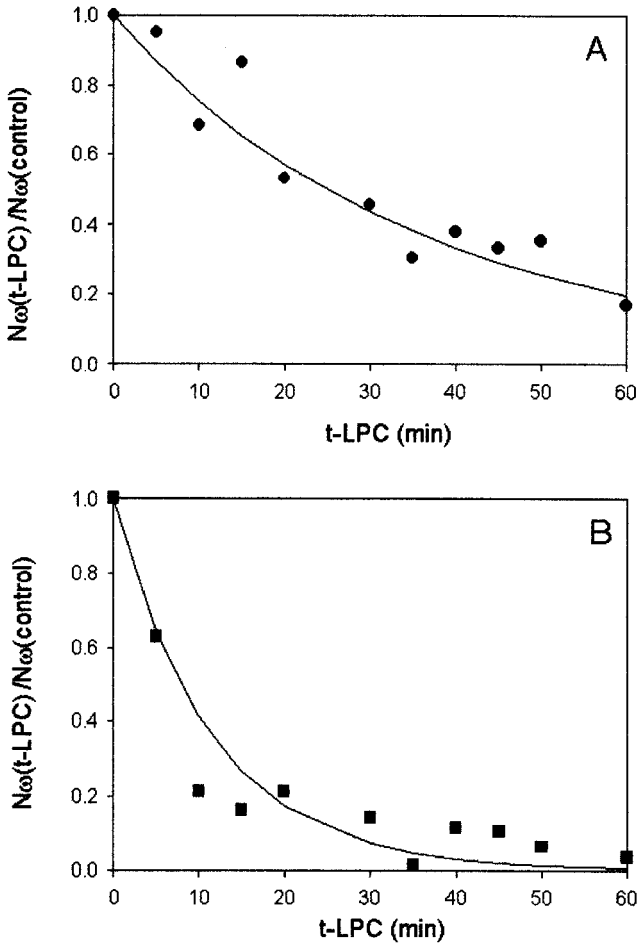

FIGURE 8 Inactivation kinetics of HA measured by Leikina et al. (2000) using HA300a cells (expressing X:31 strain of influenza HA) fusing with PKH26-labeled RBCs. Leikina et al. (2000) measured extents of fusion after incubating the HA-expressing cells bound to PKH26 labeled RBCs at pH 4.9 for 5 min in presence of LPC followed by removal of LPC at different times with (*B*) or without (*A*) addition of neuraminidase. We calculated the number of fusogenic aggregates for each value of the measured extent (shown in their Fig. 2) using steps 3 and 4 of our Fig. 1. The fusion parameters (Eq. 7) were the same as those for Fig. 6. To investigate inactivation of HA as a function of time of incubation with LPC, we normalized the number of fusogenic aggregates for each time of incubation to control (which corresponds to the number of fusogenic aggregates at pH 4.9 with 5-min incubation of the HA expressing cell—RBC complexes in presence of LPC: LPC arrests any lipid mixing, but does not affect HA conformational changes), shown by solid symbols. The normalized number of fusogenic aggregates was fitted as in Fig. 7, shown by smooth curves with (*B*) or without (*A*) neuraminidase. Effects of neuraminidase treatment were calculated using the HA-glycophorin binding reaction described in Mittal and Bentz (2001). The HA-glycophorin binding constant was taken as 10^{-2} (molecules/μm^2)$^{-1}$, and 8000 glychophorins/μm^2 were assumed on the RBC (Leikina et al., 2000; Mittal and Bentz, 2001).

Eq. B.7 gives the function used to fit the data in Fig. 2 *A* from Leikina et al. (2000) as shown by the smooth curve in

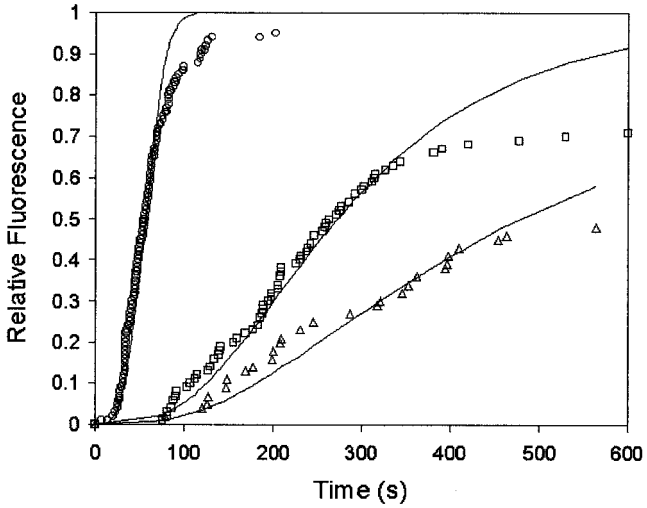

FIGURE 9 Lipid mixing between HA-cells, expressing A/Japan strain of influenza HA, and R18 labeled RBCs at different pH values. Open symbols show the lipid mixing at pH values of 4.8 (*circles*), 5.2 (*squares*), and 5.3 (*triangles*), as measured by Mittal et al. (2002) using video microscopy. Closed symbols show the fit to the data obtained from steps 3 and 4 of the kinetic model shown in Fig. 1. The primary purpose of the fitting was to find the number of fusogenic aggregates in the area of contact for each pH value. The fusion rate constants were fixed at $k_f = 1 \times 10^{-2}\ s^{-1}$, $k_p = 5 \times 10^{-4}\ s^{-1}$, and $k_1 = 3 \times 10^{-2}\ s^{-1}$. "$q$", the minimal fusion unit, was fixed at 2 and, ω, the minimal aggregate size was fixed at 8. Values of these "fusion parameters" (see Eq. 7 here) were found by Mittal and Bentz (2001) after exhaustive fitting of lipid mixing data between HA-expressing cells (same strain of HA) and R18-labeled RBCs. The only parameter fitted was number of fusogenic aggregates, and the values obtained were used to calculate the pKa for the last protonation site on each monomer of HA molecule, that activates the HA trimer for fusion (see text for details).

Fig. 8 *A* here. For experiments with addition of neuriminidase shown by Fig. 2 *B* in Leikina et al. (2000), similar calculations are done except that at the time of neuraminidase addition, all HA_{em} are treated as free, i.e., all the HA in the area of apposition are free. The smooth curve in Fig. 8 *B* shows the fit obtained for the data with addition of neuraminidase. Fitting of the data (solid symbols) in Fig. 8, *A* and *B* was done simultaneously with Eq. B8, giving us $k_{fi} = 1.9 \times 10^{-4}\ s^{-1}$, i.e., the same as found for the PR8 virions. The fit is as good as the one shown in Leikina et al. (2000) using semiempirical equations.

pKa of activation for HA from the Japan strain

Korte et al. (1999) showed that influenza A/Japan/305/57 virus does not inactivate significantly at pH 5.0 and 20°C (their Fig. 2). Fig. 9 shows the data of Mittal et al. (2002) for HAb2 cells (expressing the Japan strain of HA) fusing with R18 labeled RBCs, for which the experimental conditions were similar to Fig. 2 of Korte et al. (1999). Therefore, we investigated activation characteristics of HA from this data by neglecting the "inactivation" part in step 1 of Fig. 1. Markovic et al. (2001) have proposed that Japan HA can inactivate, in contrast to the results of Puri et al. (1990) and Korte et al. (1999), but the effect is still not significant under the conditions used in Mittal et al. (2002). With insignificant inactivation, from Eq. B3 we get $\{HA_{em}(0)\} = \{HA_{fp}(0)\}$.

Now, Eq. A11 can be used in Eq. B.2 to solve for pKa given the ratio of fusogenic aggregates at any two pH values. The video microscopy data of Mittal et al. (2002) for Japan HA expressing cells fusing with RBCs, shown by symbols in Fig. 9, was fit to LC formation in step 4 of Fig. 1, to obtain the ratios of fusogenic aggregates for the pH values of 4.8, 5.2, and 5.3. Fusion parameters for these fits were fixed at the consensus values obtained in Mittal and Bentz (2001): $k_f = 1 \times 10^{-2}\ s^{-1}$, $k_p = 5 \times 10^{-4}\ s^{-1}$, $k_1 = 3 \times 10^{-2}\ s^{-1}$, $q = 2$, and $\omega = 8$. Using other values within the respective values obtained in Mittal and Bentz (2001) would not affect the ratios of fusogenic aggregates at different pH values from the ones obtained below. The fits, shown by smooth curves in Fig. 9, gave us the number of fusogenic aggregates in the area of contact at the three pH values as N_ω (pH 4.8) $\sim$ 1100, N_ω (pH 5.2) $\sim$ 13, N_ω (pH 5.3) $\sim$ 5. Therefore, N_ω (pH 5.2)/N_ω (pH 4.8) = 0.0121 and N_ω (pH 5.3)/N_ω (pH 4.8) = 0.0046.

Solving Eqs. B.1 and B.3 using Eq. A11 for the value of pKa, the former ratio of fusogenic aggregates gave a pKa of 5.61, and the latter ratio gave a pKa of 5.68. Thus, for the Japan strain of HA, we obtained a pKa value of 5.6 to 5.7, which is very similar to what we obtained for the PR/8 virus data. Whereas the strains are different, it seems that the activation of fusion mechanism of HA is shared strongly between strains in terms of the final protonation sites on the HA trimer, which primes HA for the essential conformational change required to initiate fusion.

DISCUSSION

Previously, the data of Melikyan et al. (1995), Danieli et al. (1996), and Blumenthal et al. (1996) on HA-expressing cell lines fusing with a variety of target membranes was analyzed using the kinetic model shown in Fig. 1 (Bentz, 2000a; Mittal and Bentz, 2001). It was found that the fusogenic aggregate required at least $\omega = 8$ HAs, and of these only $q = 2$ underwent the essential conformational change for formation of the first fusion pore slowly (see tables 1 and 2 in Mittal and Bentz, 2001). Whereas, $q = 1$ or 3 could fit some of these data, only $q = 2$ could best fit all of the data from these studies.

While it was rather significant that the three independent data sets could be explained, i.e., have similar fitted parameters with a single kinetic model, there remained two important questions. First, in terms of these key fusion site architecture parameters, are the results of HA-expressing cells applicable to the virion fusing with target membranes? Second, whereas the kinetic analysis assumed a single homogeneous average surface density for each cell line, be-

cause of computational time constraints, the HA expressing cells probably have an inhomogeneous distribution of HA surface densities. The question is whether the key fusion site architecture parameters would remain largely unchanged once the distributions were incorporated into the analysis? While we are working on the second question, and the answer appears to be affirmative, our results here show, for the first time, consensus quantitative agreement on the fusion site architecture for the PR8 influenza virus and Japan-influenza HA expressing cell lines. Evidently, because the minimal aggregate size $\omega = 8$ and the minimal fusion unit $q = 2$ are obtained from ratios of fitted parameters, the effects of the distributions are not very significant.

We found that fitting all of the data in Fig. 4 simultaneously and selecting the best-fit parameter sets yielded only two convergent solutions for parameters, as opposed to ranges for parameters (Bentz 2000a; Mittal and Bentz, 2001) because more curves are being simultaneously fitted. This is an assertion of the reliability of this kinetic model. By providing more data with less experimental noise, steps 3 and 4 of the kinetic model in Fig. 1 are able to extract very robust estimates for the kinetic parameters.

The best fits for the value of minimal fusion unit from the virus data is $q = 1$ or 2. As mentioned above, it is clear that consensus value of the minimal fusion unit is 2. Whereas $q = 1$ could best fit the virus data, it does not follow the significant trend observed from the collected data. We find that as the experimental systems provide higher surface density of HAs in the area of contact, the value of the average rate of the essential conformational change of HA, k_f, increases. As can be seen from Table 1 for $q = 2$, k_f for the virus is $\sim 3\ s^{-1}$, which is one to two orders of magnitude faster than HA-expressing cells fusing with RBCs, where surface density of HA in the area of contact is increased due to accumulation resulting from HA-glycophorin binding (Mittal and Bentz, 2001). We showed that the glycophoin bound HAs could be part of the fusogenic aggregate, but like Leikina et al. (2001), we showed that the sialate bound HAs were inhibited from undergoing the essential conformational change (Mittal and Bentz, 2001). The value of k_f for the virus is four orders of magnitude faster than HA-expressing cells fusing with ganglioside containing planar bilayers (Bentz, 2000a; see table 2 in Mittal and Bentz, 2001), where very little HA binding and accumulation occurs.

The increase of k_f with HA surface density suggests cooperativity, which is not yet incorporated into the kinetic model, as its mechanism is not yet known. An increased HA surface density should yield more and larger fusogenic aggregates (Bentz, 2000a; Bentz and Mittal, 2002). Based upon our current knowledge, whereas more fusogenic aggregates would not promote any cooperativity, larger aggregates might. Recently, Markovic et al. (2001) found that the overall refolding rate of Japan, X-31 and Udorn HA increases with increasing surface density, as assayed by subsequent dithiothreitol (DTT) dissociation of the HA. The avenue of this cooperativity could well through the fusion peptides embedded in the viral or HA expressing cell bilayers (Bentz, 2000b).

Clearly, from Table 1, $q = 1$ does not fit this possible cooperativity. Günther-Ausborn et al. (2000) claimed that a single HA could cause lipid mixing between RBC and reconstituted virosomes containing HAs from two different strains, one of which was presumably inactive for fusion at the pH used. We do not believe our results support this claim for experimental and theoretical reasons. Experimental problems include that the virosomes contain residual detergent (Stegmann et al., 1987) and that the lipid mixing observed by Günther-Ausborn et al. (2000) might well have been only hemifusion of the outer monolayers, because that was not examined and accounts for over 60% of lipid mixing with HA-expressing cells and RBC at room temperature (Mittal et al., 2001). The PR8 virion data analyzed showed complete lipid mixing, because the observed dequenching required the mixing of both monolayers of the target liposomes (Shangguan et al., 1996, 1998). The theoretical problem was that their data analysis used the slope of lagtimes to predict how many HAs are at the fusion site. We have proven that lag times cannot be used to predict this number (Mittal and Bentz, 2001).

Both k_p and k_1 are an order of magnitude faster than what we previously found for HA-expressing cells fusing with target membranes. The differences might simply be HA-strain dependent. They might be because the virus has proton channels that can facilitate first conductivity (hence faster k_p) and/or the virus lipid envelope has fewer obstructions against lipid mixing (hence faster k_1) as compared with HA-expressing cells with a cytoskeleton. Because the liposomes used in Shangguan et al. (1996, 1998) were similar in composition to the planar bilayer used in Melikyan et al. (1995), the differences are not likely to be due to target membrane properties.

We have found a pKa ("pK" of activation of HA) for both PR/8 and Japan strain of HA to be 5.6 to 5.7. A key element of this analysis was assuming that inactivation of HA was not kinetically significant, based on previous findings (Puri et al., 1990; Gutman et al., 1993; Korte et al., 1999). Markovic et al. (2001) have shown that Japan HA does inactivate to some extent and proposed that the retention of fusogenic activity after low pH preincubations reflects slow activation of the strain. However, because at pH 4.9, no loss of fusion activity was found by Markovic et al. (2001) or the other studies, any inactivation of Japan HA is kinetically insignificant compared with the control experiment, which is all our analysis requires.

We believe that our finding of pKa of 5.6 to 5.7, for activation of both PR8 and Japan strains of HA provides a good incentive to investigate key histidine, aspartate, or glutamate residues common to all strains. The pKa of the histidine side chain is closest to the value we find, but

glutamate and aspartate pKs could be increased by hydrophobic or negatively charged neighbors. On the same lines, we found a pKi ("pK" of inactivation of HA) for the PR/8 strain of HA to be 4.8 to 4.9.

Recently, Han et al. (2001) did structural studies on the fusion peptide of HA in membranes. They used X31 sequence and found that Glu-15 of HA2 is repositioned in the fusogenic state of HA. However, the 15th residue of HA2 is not Glu for the three strains shown here, i.e., these structural results may not be directly applicable to the fusogenic activity of other HA strains. Korte et al. (2001) showed that whereas fusion peptides mutated at Glu-11 and Glu-15 interact with membranes very differently than wild-type fusion peptide sequence, similar mutations in HA on HA-expressing cells fusing with erythrocytes does not yield any measured difference in the fusion kinetics between mutants and wild type.

The model shown here in Fig. 1 was not conceptually designed for any single experimental system. For any given fusion measurement done with different amounts of fusogenic HA providing those fusion measurements (either by varying surface densities on HA cells or by letting HAs inactivate while blocking fusion with LPC on the same HA cells or by varying the pH of the virus fusing with liposomes), we can find precise ratios of fusogenic aggregates along with the minimal fusion unit and the relevant rate constants in steps 3 and 4 of Fig. 1. This yields differences in amounts of HAs (due to inactivation and/or protonation). This conceptualization provides us with a computationally economical approach to fit the desired data, because the number of parameters being fitted in each step of analysis is reduced, thereby allowing exhaustive fitting within practical time scales.

Fitting inactivation data of Leikina et al. (2000) (Japan HA expressing cells and RBC) and Shangguan et al. (1998) (PR8 virions and 10 mol% ganglioside PC liposomes) all gave an estimate for the rate constant for inactivation as $k_{fi} \sim 2 \times 10^{-4}\ s^{-1}$. This is about the same as $k_f \sim 1 \times 10^{-4}\ s^{-1}$ measured in Bentz (2000a) for the data of Melikyan et al. (1995), wherein Japan HA expressing cells fused with ganglioside containing bilayers. The simplest interpretation of k_f and k_{fi} is that they measure the same event, e.g., formation of the extended coiled coil, in the presence and absence of a target membrane, except that k_f also refers to a "successful" conformational change, which helps the first fusion pore to form. We would expect k_{fi} to measure the basal rate for an unbound and unaggregated HA.

In the case of RBC as the target membrane, all but two HA in a fusogenic aggregate are bound to sialates and cannot undergo the essential conformational change. Here, $k_f \sim 1 \times 10^{-2}\ s^{-1}$, and the explanation of less failure per essential conformational change given in Mittal and Bentz (2001) appears less plausible. It must be that having HAs bound to sialates within the fusogenic aggregate actually increases the rate constant for the essential conformational change for the unbound HAs by two orders of magnitude.

This might happen because the sialate bound HAs hold the fusogenic aggregate together longer and that the rate limiting step for the essential conformational change is extraction from the viral bilayer (Bentz, 2000b; Bentz and Mittal, 2000). The embedded fusion peptides create an environment conducive to the extraction of the unbound HAs fusion peptides. Perhaps the aggregate is more tightly packed, making the embedded peptides closely packed, so that extraction of the unbound HAs fusion peptide exposes only other peptide, thereby reducing the free energy, since the exposure of hydrophobic peptides to water is less expensive than exposure of acyl chains (Bentz, 2000b). The loss of fusion by the HA2 fusion peptide mutant G1V (Qiao et al., 1999) can be explained as a β-sheet aggregate (Han et al., 2001) too large or hydrophobic to be extracted. In our model, k_{fi} is the rate of loss of unaggregated HAs. If many are bound, then only the unbound ones would be lost, but then they would be in equilibrium with bound HA.

APPENDIX A: HA PROTONATION, ACTIVATION AND INACTIVATABILITY

Here we will derive the equations needed to analyze the protonation of the HA trimer. The data of Körte et al. (1997, 1999) suggest that the inactivation of PR8 and X31 HA is pH sensitive beyond that needed to activate the protein. We will treat this by assuming that HA has two independent proton binding sites on each monomer, one for activation with a dissociation constant of K_A and one for inactivation with a dissociation constant of K_1. We will assume these sites are the essential ones to be protonated for the conformational changes. Other sites with smaller dissociation constants will already have been protonated at higher pH values. Generalization is straightforward but unnecessary at this time.

Each HA trimer can be written as $HA_{i,j}$ in which i denotes the number of protons bound to the activation sites (between 0 and 3) and j denotes the number of protons bound to the inactivation sites (between 0 and 3).

$$HA_{i,j} + H^+ \overset{K_A}{\longleftrightarrow} HA_{i+1,j}$$

$$HA_{i,j} + H^+ \overset{K_1}{\longleftrightarrow} HA_{i,j+1} \qquad (A.1)$$

We will use curly brackets to denote surface density in the units of molecules per μm^2. Due to the fact that there are three identical sites, one on each monomer:

$$\{HA_{i+1,j}\} = \left(\frac{3-i}{1+i}\right)\{HA_{i,j}\}\{H^+\}/K_A$$

$$\{HA_{i,j+1}\} = \left(\frac{3-j}{1+j}\right)\{HA_{i,j}\}\{H^+\}/K_1 \qquad (A.2)$$

Solving the recursion by induction (for $i = 0{:}2$) yields:

$$\{HA_{i,j}\} = \binom{3}{i}\binom{3}{j}x_A^i x_1^j\{HA_{0,0}\} \qquad (A.3)$$

in which

$$x_A = \{H^+\}/K_A = 10^{pK_A - pH}$$
$$x_I = \{H^+\}/K_I = 10^{pK_I - pH} \quad (A.4)$$

Note that this is simply the form expected for the probability that a protein has *i* protons bound to the *A* site and *j* protons bound to the *I* site prior to normalization. For normalization or conservation of mass with $\{HA_{TOT}\}$ denoting the total HA surface density:

$$\{HA_{TOT}\} = \sum_{i=0}^{3}\sum_{j=0}^{3}\binom{3}{i}\binom{3}{j}x_A^i x_I^j\{HA_{0,0}\}$$
$$= \{HA_{0,0}\}\sum_{i=0}^{3}\binom{3}{i}x_A^i\sum_{j=0}^{3}\binom{3}{j}x_I^j$$
$$= \{HA_{0,0}\}(1+x_A)^3(1+x_I)^3 \quad (A.5)$$

so that

$$\{HA_{0,0}\} = \frac{\{HA_{TOT}\}}{((1+x_A)(1+x_I))^3} \quad (A.6)$$

The choice must be made about which species, HA_{em} and HA_{fi} are active and inactivatible due to this binding. It makes sense to require all three activation sites to be protonated because the coiled-coil formation must have all three coils (although two strands could form first). Thus, for the active fraction:

$$\{HA_{fp}\} = \sum_{j=0}^{2}\{HA_{3,j}\}$$
$$= \{HA_{TOT}\}\frac{x_A^3((1+x_1)^3 - x_1^3)}{((1+x_A)(1+x_1))^3}$$
$$= \{HA_{TOT}\}\frac{((1+x_1^{-1})^3 - 1)}{((1+x_A^{-1})(1+x_1^{-1}))^3} \quad (A.7)$$

For now, let us assume that inactivation requires all three inactivation sites to be bound. This is a weak assumption until much better inactivation data are available. This means that $[HA_{3,3}]$ is considered ready for fusion or inactivation, depending upon the relative rates. Thus, for the inactivatible fraction

$$\{HA_{fi}\} = \sum_{i=0}^{3}\{HA_{i,3}\}$$
$$= \{HA_{TOT}\}\frac{x_I^3(1+x_A)^3}{((1+x_A)(1+x_I))^3}$$
$$= \{HA_{TOT}\}\frac{1}{(1+x_I^{-1})^3} \quad (A.8)$$

Note that

$$1 + x_A^{-1} = 1 + 10^{pH - pK_A}$$
$$1 + x_I^{-1} = 1 + 10^{pH - pK_I} \quad (A.9)$$

Therefore, in summary, the initial conditions for fusion kinetics and HA inactivation are,

$$\{HA_{fp}(0)\} = \{HA_{TOT}\}\left(\frac{b-1}{ab}\right)$$
$$\{HA_{fi}(0)\} = \{HA_{TOT}\}\left(\frac{1}{b}\right)$$
$$\{HA_{na}(0)\} = \{HA_{TOT}\}\left(\frac{(a-1)(b-1)}{ab}\right)$$
$$\{HA_{init}(0)\} = \{HA_{fp}(0)\} + \{HA_{fi}(0)\}$$
$$a = (1 + 10^{pH - pKa})^3$$
$$b = (1 + 10^{pH - pKi})^3 \quad (A.10)$$

In absence of any inactivation, Eq. A7 takes the form:

$$\{HA_{em}\} = \{HA_{fp}\} = \{HA_{TOT}\}\frac{1}{(1+x_A^{-1})^3}$$

in which

$$x_A = 10^{pKa - pH} \quad (A.11)$$

APPENDIX B: HA INACTIVATION KINETICS

The typical HA inactivation experiment preincubates the virus or HA expressing cell at low pH under conditions where fusion cannot happen and then permits fusion. The reduction of the lipid mixing, compared with control, is a measure of HA inactivation. In Shangguan et al. (1998), fusion was blocked since there was no target membrane. In Leikina et al. (2000), fusion was blocked by LPC.

The model of Fig. 1 can provide a quantatative basis for inactivation kinetics by predicting the loss of fusogenic HAs, which would decrease the number of fusogenic aggregates, step 2 in Fig. 1. It may be that inactivation also proceeds from fusogenic aggregates (Markovic et al., 2001) and we have found an experimental protocol that can measure their contributions to overall inactivation. However, in the absence of this knowledge, it is simpler to ascribe all of the inactivation to the loss of activated HAs.

The number of fusogenic aggregates, N_ω in the area (δ) of contact at time *t* is given by

$$N_\omega(t) = \delta X_{\omega,0}(t)$$
$$= \delta K_{nuc}(\{HA_{em}(t)\})^\omega \quad (B.1)$$

because the nucleation reaction is assumed to be at equilibrium at all times. For the analysis of these data, a more sophisticated aggregation model is not needed. Typically, inactivation data is the amount of lipid mixing given after an incubation time, t_m, under conditions where HA can undergo conformational changes, but fusion is blocked. The inactivation data were then plotted relative to a control curve where lipid mixing was permitted from the time of lowering the pH. Because we can relate lipid mixing to the number of fusogenic aggregates in the area of contact, we can use the equation:

$$\frac{N_\omega(t_{in})}{N_\omega(\text{control})} = \left(\frac{\{HA_{em}(t_{in})\}}{\{HA_{em}(\text{control})\}}\right)^\omega \quad (B.2)$$

Note that Eq. B.3 is independent of K_{nuc}, and provides a ratio of the number of fusogenic aggregates. This is extremely important because we have

previously shown the ratio of fusogenic aggregates to be the most robust parameter of our mass action model (Bentz, 2000a; Mittal and Bentz, 2001).

Considering that aggregation of HA is not rate limiting (Bentz, 1992; Bentz, 2000a), from step 1 of Fig. 1, we get

$$\{HA_{em}(0)\} = \{HA_{fp}(0)\} + \{HA_{in}(0)\}$$

$$\{HA_{in}(0)\} = \left(\frac{1}{1 + (k_{in}/k_{em})}\right)\{HA_{fi}(0)\} \qquad (B.3)$$

Now, the experiments done at the same low pH with varying times of preincubation at that low pH will provide the same value of HA_{em} to begin with. Hence, in absence of fusion, HA_{em} will inactivate via the k_{fi} pathway as shown in Eq. 3.

From Eq. 3, in case of HA_{em} not contributing to fusion (e.g., absence of target membranes or application of LPC), it is clear that

$$\{HA_{em}(t_{in})\} = \{HA_{em}(0)\}\exp(-k_{fi} \times t_{in}) \qquad (B.4)$$

since the amount of HA in aggregates is a small fraction of the total HA, as seen from Fig. 3.

For HA expressing cells fusing with RBCs, this analysis must include our finding that of eight HAs in a fusogenic aggregate, only two are unbound to sialates and only these two free HAs can undergo the essential conformational change needed to create the fusion defect (Mittal and Bentz, 2001). HAs bound to sialates are very slow to inactivate compared with fusion kinetics (Alford et al., 1994; Leikina et al., 2000). Inactivation kinetics apply only to the free HAs in the area of apposition. Therefore, we need to actually apply the fact that the species HA_{em} capable of conformational changes for either fusion or inactivation in our model are coming only from the free HA in the area of contact. Given an HA-sialate surface binding constant of 10^{-2} (molecules/$\mu m^2)^{-1}$ estimated by Leikina et al. (2000) and Mittal and Bentz (2001) by independent methods, we calculate the surface concentrations of free and bound HAs in the area of contact, using the binding reaction:

$$HA_F + R \overset{K_\sigma}{\longleftrightarrow} HA_B$$

in which HA_F and HA_B represent the HA that are free and bound to receptor R, respectively, in the area of contact, and the binding constant for the reaction is K_σ (molecules/$\mu m^2)^{-1}$.

Therefore, because $k_{em} > 0.1\ s^{-1}$, at the prebinding step between HA expressing cells and RBCs:

$$\{HA_{em}(0)\}_{Free} = \{HA_F\} \qquad (B.5)$$

Leikina et al. (2000) applied a pulse of low pH in the presence of LPC at fusion-inhibiting concentrations after the prebinding step. Then, still in presence of LPC, but already at neutral pH, they treated (Fig. 8 *a*) or not (Fig. 8 *b*), the cells with neuraminidase (thus increasing $\{HA_F\}$). Then, at different time points after the end of low pH pulse, LPC was washed out and extents of lipid mixing were assayed. Whereas it is important to note that prior to neuraminidase treatment, the pH was brought back to neutral, for our analysis, we consider the HAs to be "primed," i.e., already activated.

From Eq. B.5, without any fusion, after incubation with LPC at low pH for time t_{in}

$$\{HA_{em}(t_{in})\}_{Free} = \{HA_{em}(0)\}_{Free}\exp(-k_{fi} \times t_{in})$$

$$= \{HA_F\}\exp(-k_{fi} \times t_{in})$$

$$\{HA_{em}(t_{in})\} = \{HA_B\} + \{HA_{em}(t_{in})\}_{Free} \qquad (B.6)$$

Note that in Eq. B.7, the former equation provides HA_{em} species that is not bound to receptor and the latter provides total HA_{em} species available after t_{in}.

Thus, fraction of free HA_{em} in the area of contact after t_{in} is given by

$$f(t_{in}) = \frac{\{HA_{em}(t_{in})\}_{Free}}{\{HA_{em}(t_{in})\}}$$

Probability that a fusogenic aggregate has two or more free HA after t_{in} is given by a binomial distribution

$$pf(t_{in}) = \sum_{i=2}^{\omega} \frac{\omega!}{(\omega - 2)!2!}\, f(t_{in})^i(1 - f(t_{in}))^{\omega - i}$$

Now, we can calculate concentrations of HA_{em} available for fusion after application of LPC for time tLPC beyond t_{in}

$$\{HA_{em}(t_{in} + t\text{LPC})\}_{Free}$$

$$= \{HA_{em}(0)\}_{Free}\exp(-k_{fi} \times (t_{in} + t\text{LPC}))$$

$$= \{HA_F\}\exp(-k_{fi} \times (t_{in} + t\text{LPC}))$$

Thus, the ratio of fusogenic aggregates for the different time points of removal of LPC is given by:

$$\frac{N_\omega(t_{in} + t\text{LPC})}{N_\omega(t_{in})} = \frac{pf(t_{in} + t\text{LPC})}{pf(t_{in})}\left(\frac{HA_{em}(t_{in} + t\text{LPC})}{HA_{em}(t_{in})}\right)^\omega \qquad (B.7)$$

We thank Dr. Leonid Chernomordik for kindly providing the original data used in Fig. 8. We also thank Drexel University for the allocation of computer time.

REFERENCES

Alford, D., H. Ellens, and J. Bentz. 1994. Fusion of influenza virus with sialic acid-bearing target membranes. *Biochemistry.* 33:1977–1987.

Armstrong, R. T., A. S. Kushnir, and J. M. White. 2000. The transmembrane domain of influenza hemagglutinin exhibits a stringent length requirement to support the hemifusion to fusion transition. *J. Cell Biol.* 151:425–437.

Bentz, J. 1992. Intermediates and kinetics of membrane fusion. *Biophys. J.* 63:448–459.

Bentz, J. 2000a. Minimal aggregate size and minimal fusion unit for the first fusion pore of influenza hemagglutinin mediated membrane fusion. *Biophys. J.* 78:227–245.

Bentz, J. 2000b. Membrane fusion mediated by coiled coils: a hypothesis. *Biophys. J.* 78:886–900.

Bentz, J., H. Ellens, and D. Alford. 1990. An architecture for the fusion site of influenza hemagglutinin. *FEBS Lett.* 276:1–5.

Bentz, J., and A. Mittal. 2000. Deployment of membrane fusion protein domains during fusion. *Cell Biol. Int.* 24:819–838.

Blumenthal, R. 1988. Cooperativity in viral fusion. *Cell Biophys.* 12:1–12.

Blumenthal, R., D. P. Sarkar, S. Durell, D. E. Howard, and S. J. Morris. 1996. Dilation of the influenza hemagglutinin fusion pore revealed by the kinetics of individual fusion events. *J. Cell Biol.* 135:63–71.

Bullough, P. A., F. M. Hughson, J. J. Skehel, and D. C. Wiley. 1994. Structure of influenza haemagglutinin at the pH of membrane fusion. *Nature.* 371:37–43.

Chernomordik, L. V., V. A. Frolov, E. Leikina, P. Bronk, and J. Zimmerberg. 1998. The pathway of membrane fusion catalyzed by influenza

hemagglutinin: restriction of lipids, hemifusion, and lipid fusion pore formation. *J. Cell. Biol.* 140:1369–1382.

Chernomordik, L. V., E. Leikina, V. Frolov, P. Bronk, and J. Zimmerberg. 1997. An early stage of membrane fusion mediated by the low pH conformation of influenza hemagglutinin depends upon membrane lipids. *J. Cell. Biol.* 136:81–93.

Danieli, T., S. L. Pelletier, Y. I. Henis, and J. M. White. 1996. Membrane fusion mediated by the influenza virus hemagglutinin requires the concerted action of at least three hemagglutinin trimers. *J. Cell Biol.* 133:559–569.

Doms, R. W., A. Helenius, and J. White. 1985. Membrane fusion activity of the influenza virus hemagglutinin. The low pH-induced conformational change. *J. Biol. Chem.* 260:2973–2981.

Duzgunes, N., M. C. Pedroso de Lima, L. Stamatatos, D. Flasher, D. Alford, D. S. Friend, and S. Nir. 1992. Fusion activity and inactivation of influenza virus: kinetics of low pH-induced fusion with cultured cells. *J. Gen. Virol.* 73:27–37.

Ellens, H., J. Bentz, D. Mason, F. Zhang, and J. M. White. 1990. Fusion of influenza hemagglutinin-expressing fibroblasts with glycophorin-bearing liposomes: role of hemagglutinin surface density. *Biochemistry.* 29:9697–9707.

Günter-Ausborn, S., P. Schoen, I. Bartholdus, J. Wilschut, and T. Stegmann. 2000. Role of hemagglutinin surface density in the initial stages of influenza virus fusion: lack of evidence for cooperativity. *J. Virol.* 74:2714–2720.

Gutman, O., T. Danieli, J. M. White, and Y. I. Henis. 1993. Effects of exposure to low pH on the lateral mobility of influenza hemagglutinin expressed at the cell surface: correlation between mobility inhibition and inactivation. *Biochemistry.* 32:101–106.

Han, X., J. H. Bushweller, D. S. Cafiso, and L. K. Tamm. 2001. Membrane structure and fusion-triggering conformational change of the fusion domain from influenza hemagglutinin. *Nat. Struct. Biol.* 8:715–720.

Korte, T., R. F. Epand, R. M. Epand, and R. Blumenthal. 2001. Role of the Glu residues of the influenza hemagglutinin fusion peptide in the pH dependence of fusion activity. *Virology.* 289:353–361.

Korte, T., K. Ludwig, F. P. Booy, R. Blumenthal, and A. Herrmann. 1999. Conformational intermediates and fusion activity of influenza virus hemagglutinin. *J. Virol.* 73:4567–4574.

Korte, T., K. Ludwig, M. Krumbiegel, D. Zirwer, G. Damaschun, and A. Herrmann. 1997. Transient changes of the conformation of hemagglutinin of influenza virus at low pH detected by time-resolved circular dichroism spectroscopy. *J. Biol. Chem.* 272:9764–9770.

Leikina, E., D. L. LeDuc, J. C. Macosko, R. Epand, R. Epand, Y. K. Shin, and L. V. Chernomordik. 2001. The 1-127 HA2 construct of influenza virus hemagglutinin induces cell-cell hemifusion. *Biochemistry.* 40: 8378–8386.

Leikina, E., I. Markovic, L. V. Chernomordik, and M. M. Kozlov. 2000. Delay of influenza hemagglutinin refolding into a fusion-competent conformation by receptor binding: a hypothesis. *Biophys. J.* 79: 1415–1427.

Markovic, I., E. Leikina, M. Zhukovsky, J. Zimmerberg, and L. V. Chernomordik. 2001. Synchronized activation and refolding of influenza hemagglutinin in multimeric fusion machines. *J. Cell Biol.* 155: 833–844.

Melikyan, G. B., W. Niles, and F. S. Cohen. 1995. The fusion kinetics of influenza hemagglutinin expressing cells to planar bilayer membranes is affected by HA surface density and host cell surface. *J. Gen. Physiol.* 106:783–802.

Mittal, A., and J. Bentz. 2001. Comprehensive kinetic analysis of influenza hemagglutinin mediated membrane fusion: role of sialate binding. *Biophys. J.* 81:1521–1535.

Mittal, A., E. Leikina, J. Bentz, and L. V. Chernomordik. 2002. Kinetics of influenza hemagglutinin-mediated membrane fusion as a function of technique. *Anal. Biochem.* 303:145–152.

Mittal, A., E. Leikina, L. V. Chernomordik, and J. Bentz. 2001. Monitoring single cell fusion kinetics from automated video fluorescence microscopy. *Mol. Biol. Cell.* 12:404A.

Nir, S., N. Duzgunes, M. C. de Lima, and D. Hoekstra. 1990. Fusion of enveloped viruses with cells and liposomes: activity and inactivation. *Cell Biophys.* 17:181–201.

Puri, A., F. P. Booy, R. W. Doms, J. M. White, and R. Blumenthal. 1990. Conformational changes and fusion activity of influenza virus hemagglutinin of the H2 and H3 subtypes: effects of acid pretreatment. *J. Virol.* 64:3824–3832.

Qiao, H., R. T. Armstrong, G. B. Melikyan, F. S. Cohen, and J. M. White. 1999. A specific point mutant at position 1 of the influenza hemagglutinin fusion peptide displays a hemifusion phenotype. *Mol. Biol. Cell.* 10:2759–2769.

Ruigrok, R. W. H., P. J. Andree, R. A. M. Hooft Van Huysduynen, and J. E. Mellema. 1984. Characterization of three highly purified influenza virus strains by electron microscopy. *J. Gen. Virol.* 65:799–802.

Ruigrok, R. W. H., P. C. J. Krijgsman, F. M. de Ronde-Verloop, and J. C. de Jong. 1985. Natural heterogeneity of shape, infectivity and protein composition in an influenza A (H3N2) virus preparation. *Virus Res.* 3:69–76.

Shangguan, T. 1995. Influenza virus fusion mechanisms. PhD Dissertation, Drexel University, Philadelphia, PA.

Shangguan, T., D. Alford, and J. Bentz. 1996. Influenza virus-liposomes lipid mixing is leaky and largely insensitive to the material properties of the target membrane. *Biochemistry.* 35:4956–4965.

Shangguan, T., D. Siegel, J. Lear, P. Axelsen, D. Alford, and J. Bentz. 1998. Morphological changes and fusogenic activity of influenza virus hemagglutinin. *Biophys. J.* 74:54–62.

Skehel, J. J., and D. C. Wiley. 1998. Coiled coils in both intracellular vesicle and viral membrane fusion. *Cell.* 95:871–874.

Stegmann, T., H. W. Morselt, F. P. Booy, J. F. van Breemen, G. Scherphof, and J. Wilschut. 1987. Functional reconstitution of influenza virus envelopes. *EMBO J.* 6:2651–2659.

Wilson, I. A., J. J. Skehel, and D. C. Wiley. 1981. Structure of the haemagglutinin membrane glycoprotein of influenza virus at 3Å resolution. *Nature.* 289:366–373.